Earth and Planetary Science Letters 524 (2019) 115717

Contents lists available at ScienceDirect

Earth and Planetary Science Letters

www.elsevier.com/locate/epsl

Vegetation and environmental changes in tropical South America from the last glacial to the Holocene documented by multiple cave sediment proxies

Valdir F. Novello [a,b,*], Francisco W. Cruz [a], Michael M. McGlue [c], Corinne I. Wong [d], Brittany M. Ward [e], Mathias Vuille [f], Rudney A. Santos [a], Plinio Jaqueto [g], Luiz C.R. Pessenda [h], Tiago Atorre [i], Ligia M.A.L. Ribeiro [a], Ivo Karmann [a], Eline S. Barreto [a], Hai Cheng [j], R. Lawrence Edwards [k], Marcos S. Paula [a], Denis Scholz [b]

[a] Instituto de Geociências, Universidade de São Paulo, São Paulo, Brazil
[b] Institut für Geowissenschaften, Johannes Gutenberg-Universität Mainz, Mainz, Germany
[c] Earth and Environmental Sciences, University of Kentucky, Kentucky, USA
[d] University of Texas, Texas, USA
[e] Boston College, Massachusetts, USA
[f] Department of Atmospheric and Environmental Sciences, University at Albany, Albany, NY, USA
[g] Instituto de Astronomia, Geofísica e Ciências Atmosféricas, Universidade de São Paulo, São Paulo, Brazil
[h] Center for Nuclear Energy in Agriculture (CENA), Universidade de São Paulo, São Paulo, Brazil
[i] Flinders University, Adelaide, Australia
[j] Institute of Global Environmental Change, Xi'an Jiaotong University, Xi'an, China
[k] Department of Earth Sciences, University of Minnesota, Minneapolis, MN, USA

ARTICLE INFO

Article history:
Received 18 April 2019
Received in revised form 13 July 2019
Accepted 17 July 2019
Available online xxxx
Editor: L. Robinson

Keywords:
paleoclimate
paleo-vegetation
speleothems
isotopes
cave sediments

ABSTRACT

$\delta^{18}O$ values in speleothems have been utilized to document past changes in South American monsoon intensity. However, changes in regional vegetation and ecosystems have not been part of this discussion, and other cave proxies such as speleothem $\delta^{13}C$ values, a useful proxy for vegetation reconstruction, have been neglected due to interpretive complexities. Here we report $\delta^{13}C$ values and $^{87}Sr/^{86}Sr$ ratios in stalagmites, together with XRF-derived elemental chemistry, $\delta^{13}C_{org}$ values and carbon content from a sedimentary profile from the same cave where the stalagmites were collected. In combination with a previously published $\delta^{18}O$ record, this enables us to clarify climate and environmental shifts that occurred between the Last Glacial Maximum and the Holocene in central South America. We show that vegetation was sparse during the last glacial period in spite of a previously inferred strong monsoon, and that changes in atmospheric pCO_2 combined with local hydrological and temperature feedbacks may have determined vegetation development during this time.

1. Introduction

Most vegetation reconstructions around the world for the Last Glacial Maximum (LGM), including South America, reveal a radical reduction of forested areas in contrast to vegetation from the Holocene period. Three main factors are likely to explain these changes: cooler temperatures, less effective precipitation, and lower levels of atmospheric CO_2 (Woillez et al., 2011). However, stable isotope records from western Amazon to southern Brazil show a coherent picture of an intense summer monsoon during the LGM, which contrasts with proxy reconstructions of monsoon strength for the early-middle Holocene (Cruz et al., 2007; Cheng et al., 2013a, 2013b; Novello et al., 2017). This suggests that water availability may not be the major driver of the vegetation changes at the transition from the LGM to the Holocene. Notably, modeling results for tropical regions indicate that the physiological effect of glacial atmospheric CO_2 levels is a key factor in explaining vegetation changes (Harrison and Prentice, 2003; Prentice and Harrison, 2009; Woillez et al., 2011), but this control is not well represented in paleoclimate and paleo-vegetation proxy data for South America. In Africa, for example, Jolly and Haxeltine (1997) used a vegetation model to test the relative impact of precipitation, temperature, and pCO_2 on tropical vegetation, and showed that when pCO_2 is decreased to glacial levels, forests are

* Corresponding author at: Instituto de Geociências, Universidade de São Paulo, São Paulo, Brazil.
E-mail address: vfnovello@gmail.com (V.F. Novello).

https://doi.org/10.1016/j.epsl.2019.115717
0012-821X/

replaced by shrubs even when water availability was high. Using the same model, Cowling et al. (2001) reported similar results for the Amazonian forest, although those authors parameterized drier conditions during the LGM for the Amazon Basin.

Open vegetation characterized by the predominance of grasses has a typical $\delta^{13}C$ signature between $-16‰$ and $-10‰$, due to the C_4 photosynthetic pathway, whereas dense vegetation characterized by trees is usually dominated by the C_3 photosynthetic pathway, with a $\delta^{13}C$ signature between $-26‰$ and $-20‰$ (Cerling, 1984). Ehleringer and Bjorkman (1977) have shown that the abundance of C_4 plants increases relative to C_3 plants at lower atmospheric CO_2 levels. Thus, it is expected that the increase in pCO_2 at the transition from the LGM to the Holocene triggered changes in the abundance of C_4 and C_3 plants. In this context, precisely dated, high resolution $\delta^{13}C$ records from stalagmites that contain the LGM-Holocene transition can be a useful tool to test this hypothesis. As an example, geochemical models considering carbonate bedrock with a $\delta^{13}C$ value of $+1‰$ predict stalagmite $\delta^{13}C$ values of $-14‰$ to $-6‰$ for caves situated beneath C_3 plant cover, whereas stalagmite $\delta^{13}C$ values of $-6‰$ to $+2‰$ are anticipated for a system dominated by C_4 vegetation (Hendy, 1971; Baker et al., 1997; McDermott, 2004). However, with few exceptions, $\delta^{13}C$ values in stalagmites have not been used as a proxy for paleo-vegetation reconstruction, due to several other factors in the karst system that can complicate the interpretation of the $\delta^{13}C$ signal (Meyer et al., 2014).

In order to interpret cave proxies and document changes in vegetation during the transition from the LGM to the Holocene, we adopted a multi-proxy approach that utilizes $\delta^{13}C$ values and $^{87}Sr/^{86}Sr$ ratios in stalagmites, combined with XRF-derived elemental chemistry, $\delta^{13}C_{org}$, total organic carbon and total inorganic carbon (carbonate) in a sedimentary profile from the same cave. We use these data to contextualize interpretations for the possible controls on vegetation change in tropical South America during this important period.

The proxies used in this study were obtained in Jaraguá cave, which is located in mid-western Brazil, a transitional region where Amazonia, the Atlantic forest, Pantanal, *Caatinga* (dry forest) and *Cerrado* (Brazilian savanna) meet. The area also serves as a moisture pathway for the South American Summer Monsoon (SASM), which connects the Amazon Basin with the La Plata Basin (the two major drainages of South America). Despite an increasing number of published paleo-rainfall and paleo-vegetation records, it remains unclear how precipitation and vegetation varied during the late Quaternary in the Neotropics in general, and mid-western Brazil in particular. Thus, a substantial knowledge gap exists with respect to climate-vegetation interactions across the LGM-Holocene transition, when global shifts in moisture distribution, temperature, and atmospheric pCO_2 are known to have occurred.

2. Cave environment

Jaraguá Cave (21°05′S, 56°35′W, ~570 m above sea level) is located in Bonito City, in the state of Mato Grosso do Sul, western Brazil (Fig. 1). This region is located along the southern border of the Pantanal, a vast and relatively pristine wetland ecosystem extending over 135,000 km^2 (Junk et al., 2006) that is internationally recognized for its biodiversity by both UNESCO (world heritage site 2000) and Ramsar (sites 602, 1270 and 1864). The climate in Bonito City is tropical, with a three-month long dry season during the austral winter (JJA) (Novello et al., 2017, 2018). The annual rainfall is ~1378 mm, with minimum monthly means of ~61, 37 and 44 mm in June, July and August, respectively, and maxima of ~151, 184 and 188 mm in November, December and January, respectively (data obtained from National Water Agency of Brazil – www.ana.gov – for the period between 1968 and 2013). Climate monitoring performed during the last seven years in this

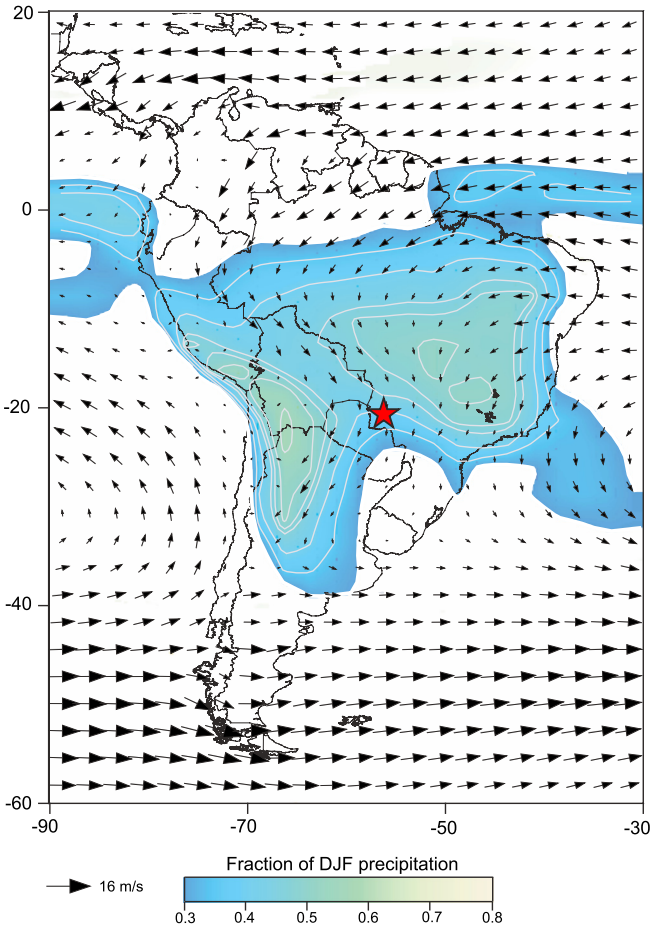

Fig. 1. Map of South America with the location of Jaraguá cave. Austral summer (DJF) 850 hPa wind field and fractional DJF precipitation. Color shading indicates regions where the fraction of total annual precipitation falling during austral summer (DJF) > 0.3, highlighting the extent of the SASM over the continent; contour interval is 0.05. Wind data is from ERA-Interim and precipitation data from GPCC, with averages calculated over the period 1979–2014. Red star indicates the location of Jaraguá cave. (For interpretation of the colors in the figure(s), the reader is referred to the web version of this article.)

area documents temperature extremes ranging from the −3 °C to 44 °C. The annual mean of 22 °C is near the average temperature of 21.4 °C inside the cave, which shows a range of 2.8 °C (Fig. S1). The relative humidity inside the cave was predominantly saturated (100%) during the monitoring period, especially towards the end of the cave (Fig. S2). Above the cave, the vegetation consists mainly of semi-deciduous savanna forest (Fig. S3).

The entrance of Jaraguá cave is located high up on a hillside (Figs. S4 and S5), which makes this setting desirable for studying ancient hilltop soils that were eroded and transported into the cave through a steep gallery (Fig. S6) and trapped in the lower part of the cave (Figs. S7 and S8). Due to the cave's location, the only possible source for sediments encountered inside the cave is the area above and surrounding the entrance (Fig. S4). At the site of deposition, a ~244 cm thick brownish, red sediment sequence was detected with ground-penetrating radar (GPR) (Fig. S9), which contrasts with the overall thin (<20 cm) soil layer above the cave today.

3. Material and methods

3.1. Trench sedimentary profile

In order to reconstruct the paleo-environment above Jaraguá cave, a 209 cm deep trench was excavated in the sediment se-

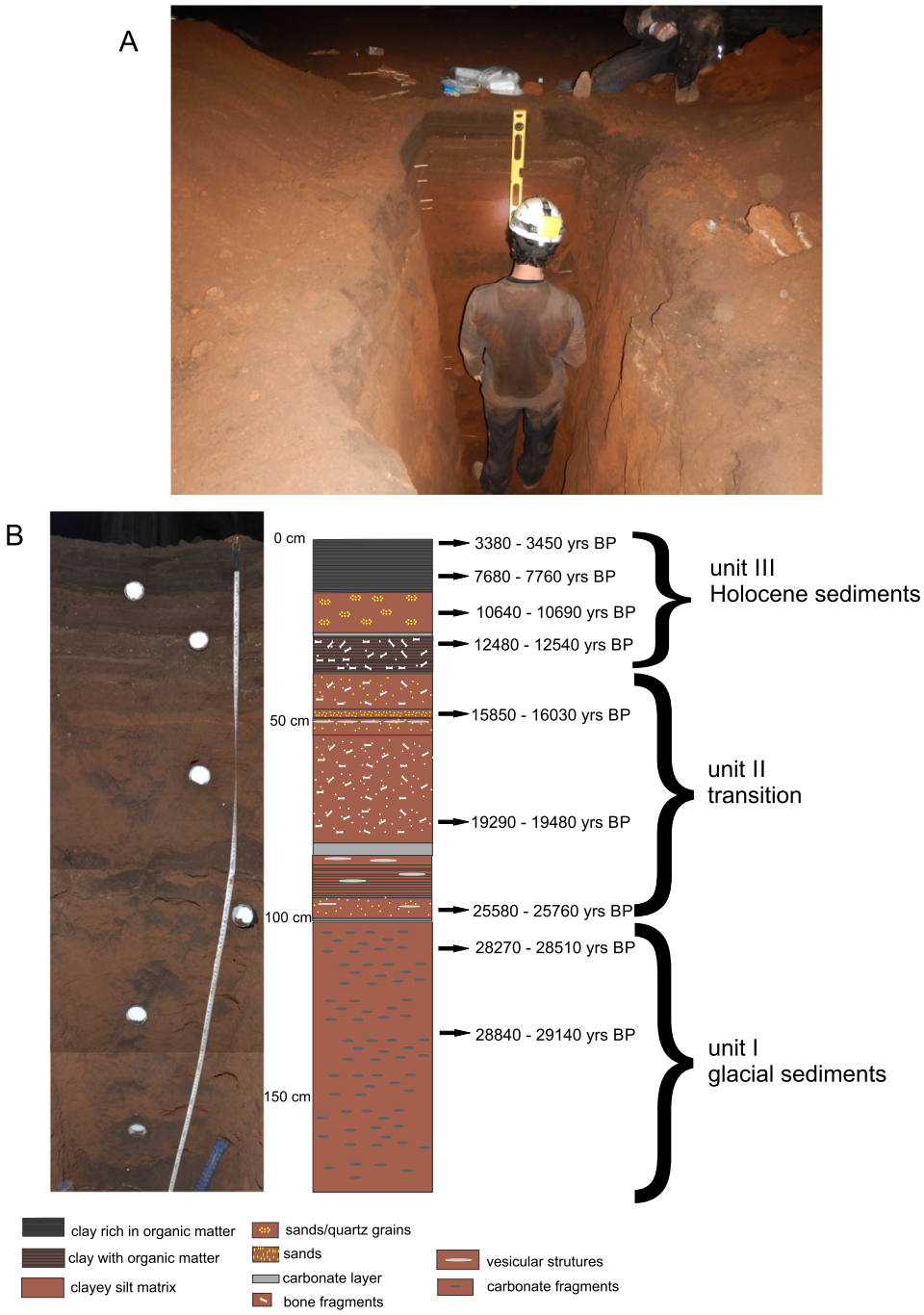

Fig. 2. (A) Trench sedimentary profile dug into the floor at the end of Jaraguá cave and the (B) schematic depositional sequence.

quence identified on the cave floor with GPR (Fig. 2). This trench was sampled in 1-cm increments for analyses of major element concentrations using energy-dispersive X-ray fluorescence (XRF), organic matter carbon isotope values ($\delta^{13}C_{org}$), and carbon content (total organic and inorganic carbon). The sediment sequence contained several indurated carbonate layers, which were excluded from the geochemical analyses performed on the unconsolidated sediments.

The chronology of the profile was established using nine ^{14}C ages measured on organic matter. The AMS ^{14}C dating was performed by Beta Analytic Incorporated. Fine-grained sedimentary organic matter was isolated through sieving, and samples were pre-treated with an acid-base-acid digestion to remove contaminants. The age model was constructed using Bacon (Blaauw and Christen, 2011), which uses millions of Markov-Chain Monte Carlo simulations to estimate accumulation rates between dated horizons. Ages were calibrated in Bacon using the SHCal13 correction (Hogg et al., 2013).

3.2. XRF analysis on the trench profile

Energy dispersive X-ray fluorescence was used to measure major and trace elements on trench sediment samples using a Bruker Tracer IV at the University of Kentucky. Sediment samples were freeze-dried, passed through a 125 µm-sieve to eliminate bone fragments and coarse detritus, and densely packed into sample holders; each sample was scanned twice for 90 s. Major element (atomic numbers 11–26) scans were run at 15.00 keV and 41.00 µA

under a 9 Torr vacuum, whereas trace elements (atomic numbers 27–51) were scanned using 40.00 keV and 35.00 μA without a vacuum. Internal consistency and machine drift were tracked by repeated scanning of the carbonaceous shale standard SARM-41. Raw counts were converted into elemental weight percentages using Bruker software and the empirical calibrations described in Rowe et al. (2012), which utilized more than 90 mudstone samples of varying chemical composition. Principal component analysis (PCA) on major element data was conducted using the software PAST (Hammer et al., 2001).

3.3. Carbon isotope analysis on trench profile sediments

Sediment samples for $\delta^{13}C_{org}$ analysis were digested for several hours at room temperature in 1 M HCl to remove carbonate and rinsed with high-purity DI water. The acid-insoluble organic fraction was freeze-dried and homogenized, and run for carbon isotope analysis using continuous flow isotope ratio mass spectrometry at the University of Kentucky. The samples were analyzed using an elemental analyzer coupled to an isotope ratio mass spectrometer through an open split interface. Carbon isotope results are expressed in δ-notation, with the per mil deviation from the VPDB standard. $\delta^{13}C = [(({}^{13}C/{}^{12}C)_{sample})/({}^{13}C/{}^{12}C)_{VPDB}) - 1] \times 1000‰$. The reproducibility of the acetanilide standard was $\leq 0.2‰$ for $\delta^{13}C_{org}$.

3.4. Total carbon on the trench profile

Total carbon data were obtained through LECO (total carbon) and carbonate coulometry (total inorganic carbon) at the University of Kentucky. For total carbon (wt.% TC), bulk samples were split, freeze-dried, and homogenized; following the addition of a combustion catalyzer (Com-Cat 502–321), samples were measured using a LECO SC-144DR device. Two synthetic carbon standards and a carbonaceous shale (SARM-41) were used to track analytical performance, and precision was better than 1.0%. Sample splits were also analyzed for total inorganic carbon (wt.% TIC) on a UIC CM5130 carbonate coulometer. Precision for that analysis was ±0.2%. The wt.% TOC value was calculated by subtracting TIC from TC.

3.5. Stalagmites

Five stalagmites (JAR4, JAR2, JAR7, JAR14 and JAR13) were utilized to compose the isotopic records of this study. All stalagmites were collected on the opposite side of the cave away from the entrance (Fig. S8). With exception of JAR2, the ages and geochronological model were published in Novello et al. (2017) for stalagmites JAR7, JAR14 and JAR13, and in Novello et al. (2018) for stalagmite JAR4. The JAR2 stalagmite is ~49 cm long and its isotopic record is composed of 505 measurements constrained by 16 ^{230}Th/U ages (Table S2). Isotopic data were linearly interpolated between the ages.

For the ^{230}Th/U analyses in stalagmite JAR2 and the carbonate layers found in the sedimentary profile, powdered carbonate was hand-drilled along the growth axis of the speleothems and spiked with a mixed ^{233}U–^{236}U–^{229}Th spike similar to that described in Edwards et al. (1987). Chemical procedures for separating uranium and thorium into different solutions were carried out at the Minnesota Isotope Laboratory and were measured using a multi-collector inductively coupled plasma mass spectrometry technique (MC-ICP-MS, Thermo-Finnigan NEPTUNE). Analytical procedures and age calculation are described in detail in Cheng et al. (2013a, 2013b).

3.6. Stalagmite $\delta^{18}O$ and $\delta^{13}C$

Stalagmite stable isotope analyses were carried out at the Stable Isotope Laboratory of the Geosciences Institute of the University of São Paulo (LES-CPGeo-IGc-USP) using a Thermo-Finnigan Delta Plus Advantage mass spectrometer. Isotope ratios are expressed in δ-notation. The reproducibility of the standard was ~0.1‰ for both $\delta^{18}O$ and $\delta^{13}C$. Approximately 100 to 200 μg of powder was drilled for each measurement along a profile following the growth axes of the stalagmites.

3.7. Stalagmite $^{87}Sr/^{86}Sr$ rations

A set of 35 ^{87}Sr/^{86}Sr analyses were performed on the five stalagmites in this study. Soils, bedrock, and drip water were collected from Jaraguá cave to characterize the potential Sr isotope signature of each member. The analyses were conducted at the Boston College Center for Isotope Geochemistry (BC-CIG). Speleothem powder (2 mg) was hand-drilled using a dental drill at ~200-yrs resolution. Dried, disaggregated soils (0.5 g) and crushed bedrock (0.25 g) were leached in 1 M ammonium acetate. All samples were processed using ion exchange methods as discussed by Montañez et al. (2000) and loaded onto outgassed single Re filaments in a TaF loading solution for analyses on an Isotopx Phoenix Thermal Ionization Mass Spectrometer (TIMS) at BC-CIG. Samples were analyzed using a dynamic measurement. The uncertainty of all ^{87}Sr/^{86}Sr ratios measured at BC-CIG is 0.000007, based on the 2σ-standard deviation of SRM987 (mean = 0.710243, $n = 42$).

3.8. Carbon isotope analysis of modern vegetation samples

Ten modern plant samples were collected above and along the flanks of the Jaraguá cave hillside, where the vegetation is predominantly an arboreal savanna assemblage. These plant samples were washed with distilled water, dried at 50 °C and pulverized. Samples (~1 mg) were analyzed for TOC and $\delta^{13}C$ values at the "Laboratório de Isótopos Estáveis" of the Center for Nuclear Energy in Agriculture (CENA) at the University of São Paulo (USP), in an ANCA SL2020 mass spectrometer. The results are expressed as a percentage of dry weight, with an analytical precision of 0.09% (TOC). The carbon isotope ratios are expressed as $\delta^{13}C$ values with respect to the VPDB standard using the δ, Analytical precision is ±0.2‰ (Pessenda et al., 2004).

4. Results

4.1. Sedimentary profile

All nine ^{14}C ages from the upper 130 cm of the profile are in correct stratigraphic order (Fig. S10 and Table S1). The youngest age obtained in the first centimeter is between 3,380 and 3,450 ^{14}C yrs BP (inclusive of error), while the oldest age at 130 cm depth is between 28,840 and 29,140 ^{14}C yrs BP. It is plausible that ancient carbon sourced from the bedrock may shift the ^{14}C ages of sedimentary organic matters to older values. However, relative agreement between the ^{14}C age-depth model and independently dated stalagmites found within the sedimentary deposit suggest that contamination, if present at all, has a minimal effect on our interpretation. One ~10 cm long stalagmite was found *in situ*, buried at ~30 cm depth in the sediment profile, and calcite layers were present at several other levels in the sediment profile. Two ^{230}Th/U analyses were performed at the top and bottom of the stalagmite, and show that it grew between 9,999 ± 37 to 9381 ± 186 yrs BP, which is close to the age predicted by the model based on the ^{14}C ages in the organic matter. One clean calcite flowstone at 170 cm was also dated by ^{230}Th/U giving an age of 43,121 ±

197 yrs BP, which is near the age expected by the high sedimentation rate at the base of the profile. The corresponding ^{230}Th/U ages are shown in Table S2. The other calcite layers in the sedimentary profile were formed by cementation, which renders dating with the ^{230}Th/U technique unreliable due to detrital Th contamination.

Three units are easily identified within the cave floor sedimentary profile: (I) red-brown glacial-aged sediments deposited before ~25,000 yrs BP from the bottom of the profile to ~100 cm; (II) a red-brown transitional unit deposited between ~25,000 yrs BP and ~12,000 yrs BP from ~100–30 cm; and (III) the brown-dark brown Holocene unit deposited in the upper 30 cm of the profile (Fig. 2). Prominent carbonate layers were found at depths of 30, 85 and 170 cm. The profile chiefly consists of horizontally stratified fine detrital sediments, consistent with an environment with relatively low energy for sediment transport. This evidence suggests a cave-floor pond depositional environment, which is consistent with these sedimentary features. However, microfossil evidence for a persistent paleolake is absent. The glacial-aged sediments (Unit I) consist of massive clayey silts with occasional carbonate concretions. The transitional Unit II also consists of massive clayey silts, but with higher concentrations of quartz sand and small mammal bone fragments. Unit II presents a darker hue of red-brown moving toward the upper contact (Fig. 2). The Holocene Unit III exhibits the darkest brown color of the entire profile, which is a result of high organic matter concentration (see section 4.4). The sedimentation rate in the Holocene period is, on average, half of the glacial period, with mean values of ~2.5 versus 5.0 cm/1000 yrs, respectively (Fig. S11).

4.2. Speleothem ^{230}Th/U-ages and δ^{18}O and δ^{13}C records

The isotope profiles of the five stalagmites from Jaraguá Cave cover the last ~28,000 yrs (Fig. 3) with the exception of two hiatuses in the JAR2 stalagmite at ~3,600–2,000 yrs BP and ~4,400–3,900 yrs BP. The full isotopic profile contains 4,133 isotopic data points that are constrained by 116 ^{230}Th/U ages, which corresponds to an average temporal resolution of ~7 yrs.

Whereas the δ^{18}O record of Jaraguá cave was published at Novello et al. (2017), we present the δ^{13}C profile here. Those datasets were produced jointly, which means that the δ^{13}C profile matches the δ^{18}O profile in terms of sample density, resolution, and chronological control (Fig. 3). The δ^{13}C values vary between −9.4 and 2.8‰, and the highest values occur during the glacial period from the oldest portion of the record until ~17,180 yrs BP (mean on the δ^{13}C values of 1.2‰). From ~17,180 yrs BP to 12,600 yrs BP, the variability of the values increases, and the mean absolute values slowly decrease. The biggest shift occurs between 12,600 and 10,800 yrs BP, when values decline from 0.8‰ to −9.0‰. During the Holocene period, the δ^{13}C values are predominantly around −8.6‰ with a maximum of the −3.6‰ at the middle Holocene (3,800 yrs BP).

4.3. Major element chemostratigraphy of the trench profile

A quantitative energy dispersive X-ray fluorescence (XRF) analysis performed on 159 discrete sediment samples from the trench profile shows considerable variability of major elements, especially across the LGM-Holocene transition. A principal component analysis was applied to the elemental data, and ~68% of the variance are explained by the first principal component (PC1) (Figs. 3 and 4). Strong positive loadings for PC1 are associated with wt.% Al, Si, Ti, Fe, and S, whereas strong negative loadings link to wt.% Ca and P (Fig. 4). Positive values characterize the time interval between ~28,000–13,600 yrs BP and negative values are predominant at ~12,900–4,350 yrs BP, with an abrupt transition occurring between these two periods (Fig. 3).

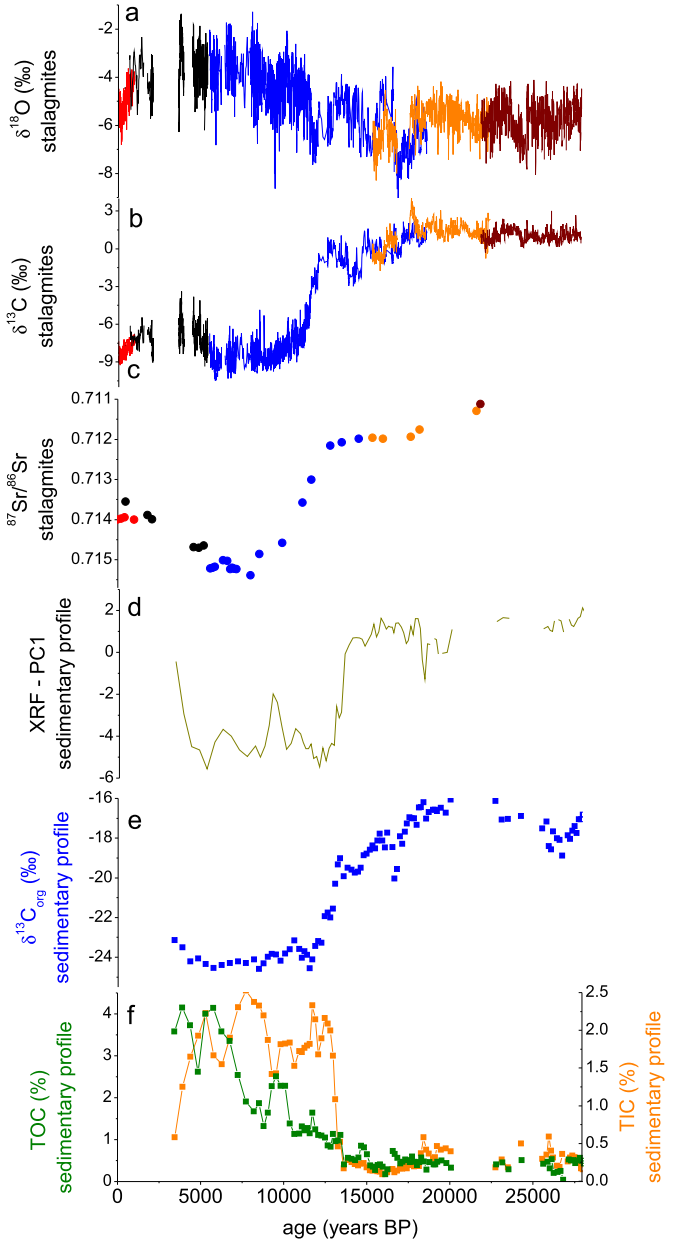

Fig. 3. Comparison between multiple proxies from Jaraguá cave. (a) δ^{18}O (‰), (b) δ^{13}C (‰) and (c) ^{87}Sr/^{86}Sr records (inverted scale) of stalagmites JAR4 (red), JAR2 (black), JAR7 (blue), JAR14 (orange) and JAR13 (wine). (d) First principal component (PC1) of the major element data from the trench profile as well as (e) δ^{13}C (‰) and (f) total organic and inorganic carbon (%) records from the trench profile.

4.4. TOC, TIC and $\delta^{13}C_{org}$ values of the trench profile

159 analyses of TOC, TIC, and $\delta^{13}C_{org}$ were performed on the trench sediments (Fig. 3). The TOC record has values around 0.5% between ~28,000 yrs BP and ~13,600 yrs BP, followed by increasing concentrations up to 3.7% in the youngest portion of the record. Similar to the TOC record, the oldest portion of the profile has TIC values that are approximately constant (0.2%) until 13,600 yrs. However, at this point, the values abruptly increase, reaching a maximum of 2.2% at 12,500 yrs BP. The TIC values oscillate around an average of 1.9% between ~12,500 yrs BP and ~4,400 yrs BP, before decreasing to 0.6% at ~3,400 yrs BP.

The $\delta^{13}C_{org}$ values in the sedimentary profile vary between −24.6% and −16.0‰ and have a striking resemblance with the

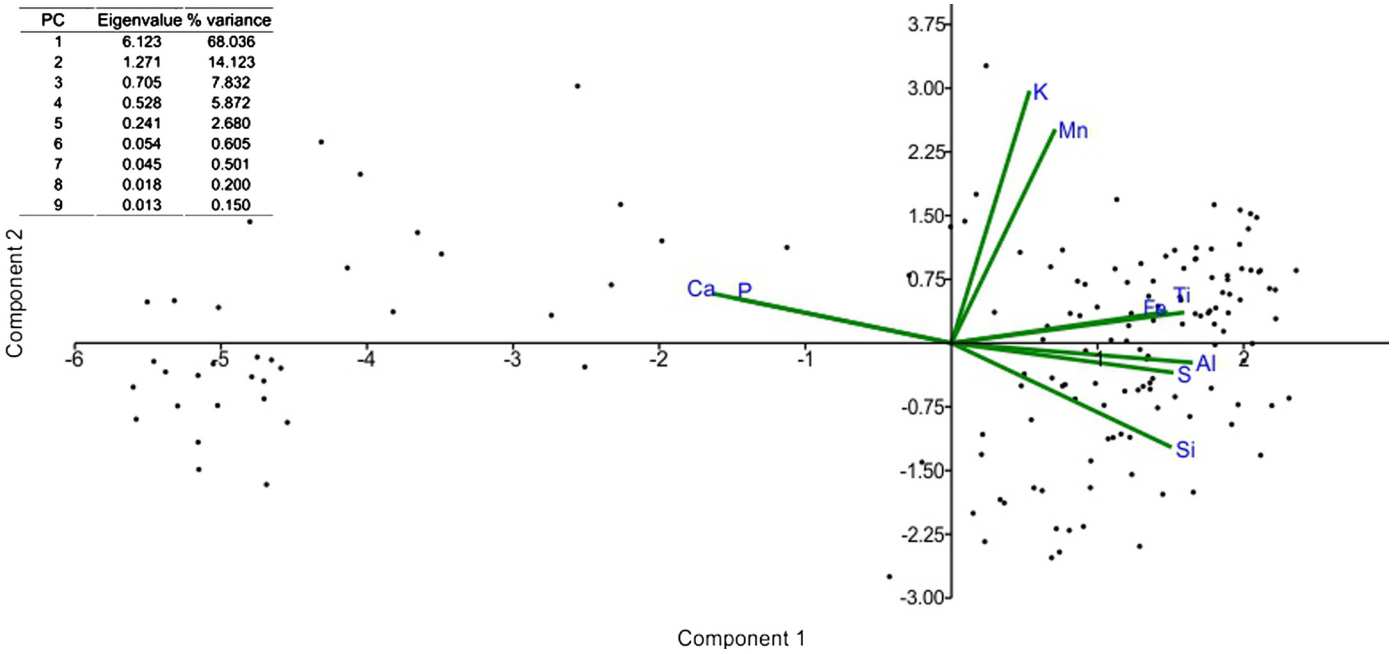

Fig. 4. Results of Principal Component Analysis from major elements measured by the dispersive x-ray fluorescence (XRF) performed on 159 discrete sediment samples from the trench profile. Weighting of each PC is in the inset panel.

variability of the $\delta^{13}C$ speleothem record (Fig. 3). Highest values occur during the glacial period until ~17,300 yrs BP (mean values of −16.9‰). From ~17,300 yrs BP to 13,200 yrs BP, the variability of $\delta^{13}C_{org}$ values increases, while mean absolute values slowly decrease. The biggest shift occurs from ~13,200 yrs BP to ~11,540 yrs BP, when values decline from −19.2‰ to −24.6‰. During the Holocene, $\delta^{13}C_{org}$ values are chiefly around −24.2‰ with a slight increase to −23.2% in the youngest portion in the record.

4.5. Speleothem $^{87}Sr/^{86}Sr$ record

The evolution of the $^{87}Sr/^{86}Sr$ values in the stalagmites has three distinct intervals. (1) The values slowly increase from 0.71111 to 0.71217 between 22,000 yrs BP and 12,800 yrs BP, (2) increases rapidly from 0.71217 to 0.71540 between 12,800 yrs BP and 8,040 yrs BP, and at this point (3) start to decrease slowly until the present, when reaches the value of 0.71398.

5. Proxy interpretations

5.1. Interpretation of the speleothem $\delta^{18}O$ values

The $\delta^{18}O$ records of Jaraguá cave have been interpreted as a proxy of SASM intensity, corroborated by isotope-enabled climate model simulations and comparisons with other paleo rainfall records, where more negative $\delta^{18}O$ values are related to a stronger monsoon and vice versa (Novello et al., 2017, 2018). Our seven-year monitoring program, which measured the local rainfall amount at the cave and its isotopic composition, also corroborates that modern local precipitation amount is related to rainfall $\delta^{18}O$ values, with more negative $\delta^{18}O$ values corresponding to higher rainfall and vice versa (Fig. S12). Thus, during the last glacial period, speleothem $\delta^{18}O$ values indicate a stronger monsoon compared to the Holocene period (Novello et al., 2017). However, recently, Wang et al. (2017) interpreted low $\delta^{18}O$ values from stalagmites from the Amazon Basin (source region from the moisture in Pantanal) as a result of less recycling of water and probably reduced plant transpiration. In this scenario, low $\delta^{18}O$ values in the stalagmites during the glacial are related with dry conditions and a less dense vegetation in the Amazon basin.

5.2. Interpretation of the speleothem $\delta^{13}C$ values

The mean $\delta^{13}C$ value (1.2‰) of the stalagmites during the glacial period (prior to 19,000 yrs BP) is substantially more positive than the mean $\delta^{13}C$ value of the Holocene section (−8.6‰) (Fig. 3). Considering that the mean $\delta^{13}C$ value of the Jaraguá cave bedrock is ~+1‰ (Table S3), the glacial $\delta^{13}C$ values of our stalagmites are in agreement with the values predicted by the geochemical models for a stalagmite growing in a cave under an environment with predominantly C_4 plants (Hendy, 1971; Baker et al., 1997). The Holocene values, in contrast, are typical for an environment dominated by trees and other C_3 vegetation.

Baker et al. (1997) suggested that degassing of CO_2 in the aquifer above the cave causing deposition of calcite before the water reached the cave (referred to as prior calcite precipitation, PCP) preferentially removes lighter carbon isotopes from the solution. This results in elevated speleothem $\delta^{13}C$ values in case of PCP (Deininger et al., 2012; Mühlinghaus et al., 2009; Hansen et al., 2019). This process should be intensified during dry periods, and the corresponding $\delta^{13}C$ values are a sensitive proxy for local hydrology. However, considering the similarities between the $\delta^{13}C$ speleothem record and the $\delta^{13}C_{org}$ values from the sedimentary profile, which are independent of the epikarst hydrology (Fig. 3 – see section 5.4), we posit that the dominant control on the $\delta^{13}C$ values of both records is the change from dominantly C_4 to C_3 plants during the transition from the LGM to the Holocene. Further evidence for this transition comes from the trench TOC, which was controlled by an increase of biogenic production of CO_2 due to the denser vegetation and the increase in soil organic matter available for transport above the cave (Fig. 3 – see section 5.4). Multiple other cave sediment proxies in our dataset reinforce this interpretation (see sections 5.3, 5.4 and 5.5).

Influences on the stalagmites $\delta^{13}C$ values by kinetic effects and/or water-rock interaction occurring under a closed or an open system in Jaraguá cave are not significant (see supplementary information).

5.3. Variability of the major elements of the trench profile

We interpret the PC1 applied to the elemental data to reflect sediment composition, which varies between siliciclastic and carbonate-rich mineralogy (see session 4.4). This interpretation is supported by a full-profile total inorganic carbon chemostratigraphy, which is strongly correlated with wt.% Ca (Fig. S15). The temporal evolution of PC1 shows a similar pattern as the speleothem $\delta^{13}C$ record, with a predominance of positive values associated with siliciclastic detritus during the glacial period and negative values during the Holocene, which reflects higher carbonate content (Fig. 3).

The siliciclastic sediment deposited in the cave during the glacial period is indicative of short residence times and sparse vegetation on hilltop soils, which we interpret to have been eroded into the cave. By contrast, lower erosion rates during the Holocene are best explained by a more dense vegetation above the cave, whose root networks reduced downslope sediment transport and allowed a thicker soil layer to accumulate. Similar relationships among vegetation assemblage changes, weathering intensity, and erosion have been documented elsewhere in the tropics (e.g., Ivory et al., 2014, 2017). Dense root networks, greater tree canopy cover (intercepting rainfall), and thicker soil profiles with higher infiltration capacity serve to reduce erosion and increase chemical weathering, which favor the accumulation of calcareous sediments within the cave sequence. Dense hillslope vegetation was potentially also responsible for the production of CO_2 and organic acids within soil pores that dissolved the bedrock, making Ca^{2+} more available to runoff into the cave during the Holocene. The relatively high concentration of P during the Holocene is likewise consistent with a denser vegetation and nutrient rich O-horizons in soils above the cave (Mischel et al., 2017), which is supported by high relative TOC in the sediment profile at this time (Fig. 3).

5.4. Interpretations of the TOC, TIC and isotope analysis on the trench profile ($\delta^{13}C_{org}$)

An increase in TOC and TIC concentrations during the Holocene period and the decrease in $\delta^{13}C_{org}$ values after the LGM are consistent with our interpretation that vegetation and thick soils developed during the Holocene. Similar to the $\delta^{13}C$ values in the stalagmites, the $\delta^{13}C_{org}$ values from the trench profile drop from -16.2 to $-24.7‰$ between ~17,600 and ~11,700 yrs BP (Fig. 3). Modern analogs from Pantanal soils show that these data likely reflect a change from C_4 grassy savanna in the Pleistocene to more organic-rich soils associated with transitional savanna vegetation and a higher relative abundance of C_3 plants (Victoria et al., 1995). The predominance of the C_3 plants over Jaraguá cave during the Holocene is consistent with its trajectory toward modern vegetation above the cave with an increase in trees. The modern arboreal savanna has plants with a mean $\delta^{13}C$ value of $-29.7‰$ ($n = 10$) (Table S4 and Fig. S16).

The shift towards more C_3 plants in the Holocene is consistent with enhanced soil profile development and less erosion above Jaraguá cave, which is very similar to the patterns inferred from the major element PC1, TOC, and TIC chemostratigraphies. The TOC concentration in the trench profile changes more gradually than the major element PC1 and TIC, which both abruptly shift across the Pleistocene-Holocene transition. By contrast, the peak in TOC is achieved in the middle Holocene, following step-wise increases beginning in the early Holocene. Soil organic carbon and its depth distribution are controlled by climate (temperature, precipitation amount and seasonality), vegetation, and clay content (Jobbágy and Jackson, 2000). The gradual increase in TOC is consistent with the progressive development of a dense vegetation and stabilized soil profiles above the cave during the Holocene. Thus, as soil profiles developed and C_3 vegetation progressively established, the production of organic matter increased.

5.5. Interpretation of the speleothem $^{87}Sr/^{86}Sr$ record

Speleothem $^{87}Sr/^{86}Sr$ ratios directly record the Sr isotopic composition of cave water and its variations reflect changes in the relative contribution of distinct Sr sources (e.g., soil and bedrock) that have different $^{87}Sr/^{86}Sr$ signatures (Banner et al., 1997; Wortham et al., 2017; Weber et al., 2018).

The mean $^{87}Sr/^{86}Sr$ value (0.71486) of six soil samples above Jaraguá Cave is significantly higher than the mean bedrock value (0.70993). Thus, the range of stalagmite and dripwater values are constrained by the values of these two end-members (Fig. S17).

Infiltrating water acquires an initial $^{87}Sr/^{86}Sr$ signature from the soils above the cave and subsequently, the $^{87}Sr/^{86}Sr$ ratio of the bedrock by water-rock interaction (Wortham et al., 2017; Ward et al., 2019). For systems, where the soil and bedrock have different $^{87}Sr/^{86}Sr$ signatures, the $^{87}Sr/^{86}Sr$ ratios may reflect changes in the relative contribution of the two end-members or the amount of water–rock interaction, which is related to the residence time of the percolating water into the cave (Weber et al., 2018). Our multi-proxy data suggest that the soil cover was very thin or absent above Jaraguá cave during the last glacial period. Therefore, only a low contribution of soil $^{87}Sr/^{86}Sr$ to the infiltrating water and the speleothems is expected during this period. Our $^{87}Sr/^{86}Sr$ speleothem record, which shows low (near bedrock) values during the glacial period, strongly supports this interpretation (Fig. 3). The increase in the $^{87}Sr/^{86}Sr$ ratio of the speleothem at the transition from the LGM to the Holocene is simultaneous with the drop of the speleothem $\delta^{13}C$ values, which confirms that soil thickness and vegetation density above the cave increased by the early Holocene.

Alternatively, $^{87}Sr/^{86}Sr$ values in the speleothems could reflect changing amounts of water–rock interaction in response to variations in local hydrology. In such a scenario, longer water residence time during dry periods could enable enhanced water-rock interaction and greater incorporation of Sr from the bedrock in the infiltrating water (Ward et al., 2019). Considering this hypothesis, the low $^{87}Sr/^{86}Sr$ value recorded in our speleothems would indicate locally drier conditions during the last glacial period, changing to wetter conditions at the same time as vegetation became denser and switched from C_4 to C_3-dominated vegetation, as indicated by the $\delta^{13}C$ values of the speleothems and the sedimentary profile. Dry glacial conditions at Jaraguá cave are apparently inconsistent with speleothem the $\delta^{18}O$ data, which suggest a more intense monsoon during the LGM relative to the Holocene. However, $\delta^{18}O$ values are a proxy for integrated atmospheric processes related to moisture transport upstream and are not exclusively an indicator of local hydrology (Ward et al., 2019).

6. Discussion

6.1. The environmental transition between the last glacial and the Holocene

The proxy datasets from Jaraguá cave provide evidence that the paleoenvironment was very different between the last glacial and the Holocene periods. The $\delta^{13}C$ and $^{87}Sr/^{86}Sr$ records from the stalagmites show that the environment changed abruptly between ~12,600 and 10,200 yrs BP (Fig. 3 and Fig. S18), while the records from the sedimentary profile (major elements, $\delta^{13}C_{org}$ values and TIC) document this transition between ~13,600 and 11,800 yrs. These differences can be explained by the variable sensitivity of each proxy archive and the geochronological models: (i) the geochronological model of the stalagmites, based on 116 U/Th ages, is more precise and accurate than the sedimentary profile,

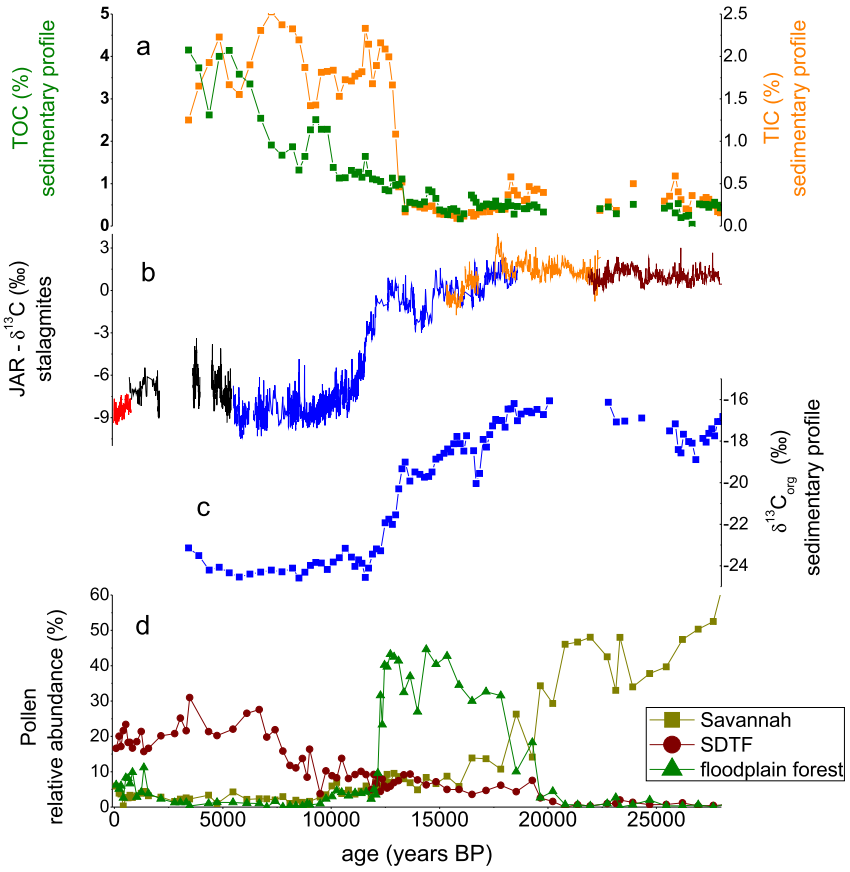

Fig. 5. Comparison between the proxies of Jaraguá cave with abundance of major vegetation groups inferred from pollen data from Laguna La Gaiba (Whitney et al., 2011; Fornace et al., 2016). (a) total organic and inorganic carbon (%) records from the trench profile (b) $\delta^{13}C$ record from the stalagmites of Jaraguá cave (this study), (c) $\delta^{13}C$ record from the sedimentary profile of Jaraguá cave (this study) and (d) abundance of major vegetation groups from pollen. Savannah includes graminoids, herbs. SDTF, seasonally dry tropical forest.

whose age-depth model consists of nine ^{14}C ages; (ii) the growth rate of the stalagmites is more constant than sediment accumulation rates on the cave floor, and (iii) the contribution of the ancient carbon from the bedrock may have shifted ^{14}C ages in the organic matter to slightly older values.

The increase of the speleothem $\delta^{13}C$ and sedimentary $\delta^{13}C_{org}$ values indicates that C_4 plants started to be replaced by C_3 plants at ~20,000 yrs BP, and this process was accentuated between 12,600 and 10,800 yrs BP (following the speleothem geochronology). At approximately the same time, the major elements PC1 and the TIC data indicate that detrital sediment composition within the cave changed. Together, these data provide evidence for changes in weathering and erosion above the cave that are best explained by a major transition in vegetation change. The increase of speleothem $^{87}Sr/^{86}Sr$ values indicates that the soil started to accumulate together with the changes in vegetation. However, soil organic matter development occurred more slowly, which controlled the gradual increase of TOC in cave floor sediments over much of the Holocene (Fig. 3).

In summary, the paleoenvironment of our study site during the last glacial period was characterized as one with very thin or absent, organic-poor hilltop soils with sparse C_4 vegetation (grasses) that were susceptible to downslope erosion. This paleoenvironment drastically changed to thicker, more organic-rich hilltop soils that were stabilized by a denser C_3 vegetation in the Holocene. This environment persisted through much of the Holocene, and the final outcome of this evolution is captured in pictures of the Jaraguá cave exterior today (Figs. S3 and S5).

Relative pollen abundance from Laguna La Gaiba (Whitney et al., 2011; Fornace et al., 2016), located at the western border of Pantanal ~370 km from our study site indicates the predominance of savannah (including grasses and herbs) and floodplain vegetation during the glacial period, which were replaced by seasonal dry tropical forest (SDTF) after 11,900 yrs BP. Although Laguna La Gaiba is strongly influenced by its proximity to the Paraguay River (McGlue et al., 2011), the vegetation change from savannah to SDTF is consistent and coeval with the transition from C_4 (grasses) to C_3 (trees) plants documented by the stalagmite $\delta^{13}C$ values and by the $\delta^{13}C_{org}$ values from the sedimentary profile of Jaraguá cave (Fig. 5). Similarly, the progressive development of the SDTF is aligned with the gradual increase in TOC from the cave (Fig. 5). These resemblances between the study sites indicates that the vegetation changes documented by the Jaraguá cave records were not simply a function of the local kart system.

Three possible causes can explain the change in environment at the transition from the LGM to the Holocene: hydrological variability, changes in temperature, and changes atmospheric CO_2. Each forcing will be discussed in the following sections.

6.2. Hydrological variability

The speleothem $\delta^{18}O$ record of Jaraguá cave indicates high monsoon intensity during the last glacial period and a weaker monsoon during the early to mid-Holocene (Novello et al., 2017), which is consistent with records for much of tropical South America over the same time period, including the western Amazon (Cheng et al., 2013a, 2013b), tropical Andes (Baker et al., 2001) and southern Brazil (Cruz et al., 2007). Considering these data, we conclude that changes in the summer monsoon cannot be the main driver for paleoenvironmental changes at Jaraguá cave. However,

if the local hydrology is not closely associated with the summer monsoon (Ward et al., 2019), and the $^{87}Sr/^{86}Sr$ record from Jaraguá cave is interpreted as a signal of bedrock residence time, relatively dry conditions could be interpreted for the last glacial period. Dry conditions during the last glacial period are in agreement with the hypothesis of Wang et al. (2017) for $\delta^{18}O$ values and with the interpretation of speleothem $\delta^{13}C$ values in Jaraguá cave as a proxy for local hydrology. Thus, drier conditions during the last glacial and a wetter Holocene period could be responsible for the environmental changes documented in Jaraguá cave at the transition. However, this scenario fails to adequately explain the linkages between monsoon intensity and the absolute differences in $\delta^{18}O$ values between the last glacial and Holocene periods.

6.3. Changes in temperature

Although the current mean annual temperature in Bonito city is ~22 °C, below-freezing temperatures are not uncommon during winter, as was, for instance, registered by our temperature logger on 30 July 2017, when temperatures fell to −3 °C (Fig. S1). It is likely that the proxy-inferred ~4 °C reduction in temperature in the Pantanal during the last glacial (Punyasena et al., 2008; Whitney et al., 2011) enhanced the frequency and amplitude of cold episodes, which in turn increased the thermal stress on vegetation. In fact, the vegetation shift and soil stabilization, as documented in the $\delta^{13}C_{org}$ values of the trench sediments and in the $\delta^{13}C$ values of the speleothems, occurred simultaneously with the increase in southern hemisphere temperature documented in the ice core record from Antarctica (Fig. 6). Cooling could also have reduced evapotranspiration rates and increased vegetation stress expected from the reduction of atmospheric pCO_2 during the glacial period.

If the pCO_2 is unchanged, C_4 plants tend to be favored over C_3 plants in warm and dry climates and, conversely, C_3 plants tend to be favored over C_4 plants in cold climates, such as the last glacial (Collatz et al., 1998). However, at tropical localities like Jaraguá cave, a substantial expansion of C_4 vegetation during the LGM has been predicted by models and verified by pollen data, despite cooler temperatures (Collatz et al., 1998; Whitney et al., 2011). Thus, colder temperatures at our study site during the last glacial could have increased the thermal stress on vegetation and inhibited soil organic matter production, but may not have been responsible for changes in the type of vegetation (C_4 versus C_3) during the transition between the LGM and the Holocene.

6.4. Changes in atmospheric pCO_2

As temperature, atmospheric pCO_2 substantially increased at the transition from the LGM to the Holocene, simultaneously with the shifts documented by the $\delta^{13}C_{org}$ values of the cave trench sediments and the $\delta^{13}C$ values of the speleothems from Jaraguá cave (Fig. 6). C_4 plants (higher $\delta^{13}C$ values) are physiologically adapted to low atmospheric pCO_2 due to a mechanism that concentrates CO_2 near the chloroplasts. Therefore, these plants are not significantly influenced by changes in atmospheric pCO_2. On the other hand, photosynthesis in C_3 plants is hindered by low atmospheric pCO_2 because of the competition between CO_2 and O_2 in enzymes responsible for fixation of both molecules (Prentice and Harrison, 2009). Thus, the observed evolution of vegetation from the Glacial to the Holocene and the predominance of C_3 over C_4 plants, which is indicated by the proxy evidence during the Holocene, probably resulted from the increase of atmospheric pCO_2 that occurred during this transition.

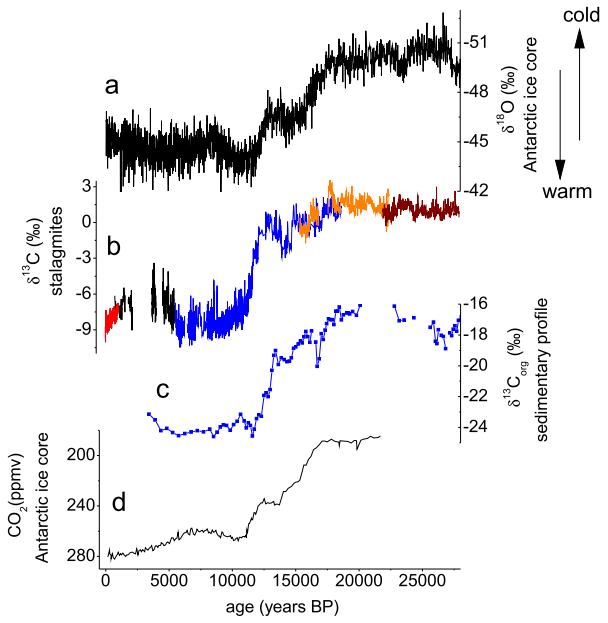

Fig. 6. Comparison between $\delta^{13}C$ records from Jaraguá cave with global records. (a) EDML ice core $\delta^{18}O$ record from Antarctica (EPICA Community Members, 2010), (b) $\delta^{13}C$ record from the stalagmites of Jaraguá cave (this study), (c) $\delta^{13}C$ record from the sedimentary profile (trench) of Jaraguá cave (this study) and (d) atmospheric pCO_2 record from Antarctic ice core (Monnin et al., 2004). Note that the scale of the y-axis of both Antarctic records is reversed.

6.5. Feedbacks between forcings

In summary, the increase of the atmospheric CO_2 explains the environmental changes that occurred between the last glacial period and the Holocene. However, vegetation patterns are not only influenced by pCO_2. Rather, plant composition is a complex function of feedbacks among pCO_2, temperature and precipitation. The sensitivity of vegetation to a specific change in pCO_2 depends on the climate state (rainfall and temperature conditions) reached under the preceding CO_2 level (Woillez et al., 2011). It is known from Jaraguá $\delta^{18}O$ data that monsoon rainfall was impacted by abrupt millennial-scale climate events, such as Dansgaard-Oeschger cycles, Heinrich events, and the Younger Dryas, all of which occurred at the end of the last glacial period (Novello et al., 2017). These abrupt changes could have resulted in transient changes in both rainfall amount and seasonality, which in turn crossed a threshold for vegetation changes favored under the higher atmospheric pCO_2 of the Holocene.

7. Conclusions

$\delta^{13}C$ values from the stalagmites and the trench sedimentary profile from Jaraguá cave are most consistent with a C_4-dominated vegetation during the last glacial period, in contrast to a vegetation dominated by C_3 plants during the Holocene. We posit that the increase in atmospheric pCO_2 during the transition from the LGM to the Holocene, together with feedbacks from temperature and precipitation, was responsible for the change in vegetation above Jaraguá cave. Dense C_3 vegetation was responsible for soil stabilization above the cave, which led to an increase in stalagmite $^{87}Sr/^{86}Sr$ values, due to more radiogenic Sr derived from the soil. The stable soil cover above the cave during the Holocene favored the production of soil organic matter, which was responsible for changes in cave sediment mineralogy and carbon content inferred from major element and organic proxies.

Rainfall amount and temperature seem to have played a secondary role for the environmental changes of the karst system

where Jaraguá cave is situated. However, it remains unclear how the local hydrology operated at the cave site during the last glacial period. The paleo-environmental sensitivities of multiple proxies established at our site may prove to be relevant for future paleoclimatic interpretations from speleothems together with karstic clastic sediment proxies around the world.

Author contributions

V.F.N. sampled the speleothems and the trench sedimentary profile, performed the isotopes analyses in the speleothems, geochronology, designed the experiment and prepared the manuscript with direct help from M.M., F.W.C., C.I.W. and M.V.; M.M. performed the isotope analyses in the trench sediments, the XRF measurements and the carbon analyses; C.W. and B.M.W. provided the Sr isotopes analyses; I.K. co-directed the project; R.S., P.J. and L.M.A.R. assisted in the sampling of the trench profile and preparation of samples; L.C.R.P. performed the $\delta^{13}C$ analyses in the leaves. T.A. performed the scanning in the cave floor with GRP; M.S.P. assisted during field work and lab procedures; D.S. assisted on the interpretations; R.L.E., H.C., L.X. and E.S.B. assisted with the $^{230}Th/U$ analyses.

Competing interests

The authors declare no competing financial interests.

Acknowledgements

We thank Alyne Barros and Osmar Antunes for their support during the stable isotope data acquisition at the University of São Paulo. We are grateful to ICMBio for permission to collect stalagmite samples. This work was supported by the São Paulo Research Foundation (FAPESP) (grants 2016/00299-4 to I.K.; 2012/03942-4, 2014/10095-1, 2015/08351-2, 2016/15807-5, 2017/23687-2 and 2018/12285-3 fellowships to V.F.N.; 2016/24870-2 fellowship to P.J.; 2012/50260-6, 2013/50297 and 2017/50085-3 PIRE NSF-FAPESP to F.W.C.), the US National Science Foundation (NSF) grants AGS-1303828 and OISE-1743738 to M.V., NSF-AGS 1602962 to C.I.W. and 1103403 to R.L.E. and H.C., as well as German Research Foundation grants SCHO 1274/9-1 and SCHO 1274/11-1 to D.S. We thank Bronwen S. Whitney for providing the pollen assemblage records. Thorough and constructive comments from two anonymous reviewers were very helpful to improve the manuscript.

Appendix A. Supplementary material

Supplementary material related to this article can be found online at https://doi.org/10.1016/j.epsl.2019.115717.

References

Baker, A., Ito, E., Smart, P.L., McEwan, R.F., 1997. Elevated and variable values of ^{13}C in speleothems in a British cave system. Chem. Geol. 136, 263–270. https://doi.org/10.1016/S0009-2541(96)00129-5.

Baker, P.A., Seltzer, G.O., Fritz, S.C., Dunbar, R.B., Grove, M.J., Tapia, P.M., Cross, S.L., Rowe, H.D., Broda, J.P., 2001. The history of South American tropical precipitation for the past 25,000 years. Science 291, 640–643. https://doi.org/10.1126/science.291.5504.640.

Blaauw, M., Christen, J.A., 2011. Flexible paleoclimate age-depth models using an autoregressive gamma process. Bayesian Anal. 6 (3), 457–474.

Cerling, T.E., 1984. The stable isotopic composition of modern soil carbonate and its relationship to climate. Earth Planet. Sci. Lett. 71, 229–240.

Cheng, H., Sinha, A., Cruz, F.W., Wang, X., Edwards, R.L., d'Horta, F.M., Ribas, C.C., Vuille, M., Stott, L.D., Auler, A.S., 2013a. Climate change patterns in Amazonia and biodiversity. Nat. Commun. 4, 1411–1416. https://doi.org/10.1038/ncomms2415.

Cheng, H., Edwards, R.L., Shen, C-C., Polyak, V.J., Asmerom, Y., Woodhead, J., Hellstrom, J., Wang, Y., Kong, X., Spötl, C., Wang, X., Alexander Jr, E.C., 2013b. Improvements in ^{230}Th dating, ^{230}Th and ^{234}U half-life values, and U–Th isotopic measurements by multicollector inductively coupled plasma mass spectrometry. Earth Planet. Sci. Lett. 82, 371. https://doi.org/10.1016/j.epsl.2013.04.006.

Collatz, G.J., Berry, A., Clark, J.S., 1998. Effects of climate and atmospheric CO_2 partial pressure on the global distribution of C^4 grasses: present, past, and future. Oecologia 114, 441–454.

Cowling, S.A., Maslin, M.A., Sykes, M.T., 2001. Paleovegetation simulations of Lowland Amazonia and implications for neotropical allopatry and speciation. Quat. Res. 149, 140–149. https://doi.org/10.1006/qres.2000.2197.

Cruz, F.W., Burns, S., Jercinovic, M., Karmann, I., Sharp, W., Vuille, M., 2007. Evidence of rainfall variations in Southern Brazil from trace element ratios (Mg/Ca and Sr/Ca) in a Late Pleistocene stalagmite. Geochim. Cosmochim. Acta 71, 2250–2263. https://doi.org/10.1016/j.gca.2007.02.005.

Deininger, M., Fohlmeister, J., Scholz, D., Mangini, A., 2012. Isotope disequilibrium effects: the influence of evaporation and ventilation effects on the carbon and oxygen isotope composition of speleothems – a model approach. Geochim. Cosmochim. Acta 96, 57–79.

Edwards, R.L., Chen, J., Wasserburg, G., 1987. ^{238}U–^{234}U–^{230}Th–^{232}Th systematics and the precise measurements of time over the past 500,000 years. Earth Planet. Sci. Lett. 81 (2–3), 175–192.

Ehleringer, J., Bjorkman, O., 1977. Quantum yields for CO_2 uptake in C3 and C4 plants. Plant Physiol. 59, 86–90. https://doi.org/10.1104/pp.59.1.86.

EPICA Community Members, 2010. Stable Oxygen Isotopes of Ice Core EDML. PANGAEA.

Fornace, K.L., Whitney, B.S., Galy, V., Hughen, K.A., Mayle, F.E., 2016. Late quaternary environmental change in the interior South American tropics: new insight from leaf wax stable isotopes. Earth Planet. Sci. Lett. 438, 75–85.

Hammer, Ø., Harper, D.A., Ryan, P.D., 2001. Past: paleontological statistics software package for education and data analysis. Palaeontol. Electron. 4 (1), 1–9. https://doi.org/10.1016/j.bcp.2008.05.025.

Hansen, M., Scholz, D., Schöne, B.R., Spötl, C., 2019. Simulating speleothem growth in the laboratory: determination of the stable isotope fractionation ($\delta^{13}C$ and $\delta^{18}O$) between H_2O, DIC and $CaCO_3$. Chem. Geol. 509, 20–44.

Harrison, S.P., Prentice, C.I., 2003. Climate and CO_2 controls on global vegetation distribution at the last glacial maximum: analysis based on palaeovegetation data, biome modelling and paleoclimate simulations. Glob. Change Biol. 9, 983–1004.

Hendy, C.H., 1971. The isotopic geochemistry of speleothems I. The calculation of the effects of different modes of formation on the isotopic composition of speleothems and their applicability as palaeoclimatic indicators. Geochim. Cosmochim. Acta 85, 801–824.

Hogg, A.G., Hua, Q., Blackwell, P.G., Niu, M., Buck, C.E., Guilderson, T.P., Heaton, T.J., Palmer, J.G., Reimer, P.J., Reimer, R.W., Turney, C.S.M., Zimmerman, S.R.H., 2013. SHCal13 Southern Hemisphere calibration, 0–50,000 years cal BP. Radiocarbon 55 (4), 1889–1903. https://doi.org/10.2458/azu_js_rc.55.16783.

Ivory, S.J., McGlue, M.M., Ellis, G.S., Lézine, A.M., Cohen, A.S., Vincens, A., 2014. Vegetation controls on weathering intensity during the last deglacial transition in southeast Africa. PLoS ONE 9 (11), e112855.

Ivory, S.J., McGlue, M.M., Ellis, G.S., Boehlke, A., Lézine, A.M., Vincens, A., Cohen, A.S., 2017. East African weathering dynamics controlled by vegetation-climate feedbacks. Geology 45 (9), 823–826.

Jobbágy, E.G., Jackson, R.B., 2000. The vertical distribution of soil organic carbon and its relation to climate and vegetation. Ecol. Appl. 10 (2), 423–436.

Jolly, D., Haxeltine, A., 1997. Effect of low glacial atmospheric CO_2 on tropical African montane vegetation. Science 276, 786–789.

Junk, W.J., Brown, M., Campbell, I.C., Finlayson, M., Gopal, B., Ramberg, L., Warner, B.G., 2006. The comparative biodiversity of seven globally important wetlands: a synthesis. Aquat. Sci. 68, 400–414. https://doi.org/10.1007/s00027-006-0856-z.

McGlue, M.M., Silva, A., Corradini, F.A., Zani, H., Trees, M.A., Ellis, G.S., Parolin, M., Swarzenski, P.W., Cohen, A.S., Assine, M.L., 2011. Limnogeology in Brazil's "forgotten wilderness": a synthesis from the large floodplain lakes of the Pantanal. J. Paleolimnol. 46 (2), 273–289.

Meyer, K.W., Feng, W., Breecker, D.O., Banner, J.L., Guilfoyle, A., 2014. Interpretation of speleothem calcite $\delta^{13}C$ variations: evidence from monitoring soil CO_2, drip water, and modern speleothem calcite in central Texas. Geochim. Cosmochim. Acta 142, 281–298.

McDermott, F., 2004. Palaeo-climate reconstruction from stable isotope variations in speleothems: a review. Quat. Sci. Rev. 23, 901–918. https://doi.org/10.1016/j.quascirev.2003.06.021.

Mischel, S.A., Scholz, D., Spötl, C., Jochum, K.P., Schröder-Ritzrau, A., Fiedler, S., 2017. Holocene climate variability in Central Germany and a potential link to the polar North Atlantic: a replicated record from three coeval speleothems. Holocene 27, 509–525.

Monnin, E., Steig, E.J., Siegenthaler, U., Kawamura, K., Schwander, J., Stauffer, B., Stocker, T.F., Morse, D.L., Barnola, J-M., Bellier, B., Raynaud, D., Fischer, H., 2004. Evidence for substantial accumulation rate variability in Antarctica during the Holocene, through synchronization of CO_2 in the Taylor Dome, Dome C and DML ice cores. Earth Planet. Sci. Lett. 224, 45–54. https://doi.org/10.1016/j.epsl.2004.05.007.

Montañez, I.P., Osleger, D.A., Banner, J.L., Mack, L.E., Musgrove, M., 2000. Evolution of the Sr and C isotope composition of Cambrian oceans. GSA Today 10 (5), 1–5.

Mühlinghaus, C., Scholz, D., Mangini, A., 2009. Modelling fractionation of stable isotopes in stalagmites. Geochim. Cosmochim. Acta 73, 7275–7289.

Novello, V.F., Cruz, F.W., Vuille, M., Stríkis, N.M., Edwards, R.L., Cheng, H., Emerick, S., De Paula, M.S., Li, X., Barreto, E.D.S., Karmann, I., Santos, R.V., 2017. A high-resolution history of the South American Monsoon from last glacial maximum to the Holocene. Sci. Rep. 7, 44267. https://doi.org/10.1038/srep44267.

Novello, V.F., Cruz, F.W., Moquet, J.S., Vuille, M., de Paula, M.S., Nunes, D., Edwards, R.L., Cheng, H., Karmann, I., Utida, G., Stríkis, N.M., Campos, J.L.P.S., 2018. Two millennia of South Atlantic convergence zone variability reconstructed from isotopic proxies. Geophys. Res. Lett. 45 (10), 5045–5051. https://doi.org/10.1029/2017GL076838.

Pessenda, L.C.R., De Souza, A., Eli, S., Gouveia, M., Aravena, R., Boulet, R., 2004. Vegetation dynamics during the late Pleistocene in the Barreirinhas region, Maranhão State, northeastern Brazil, based on carbon isotopes in soil organic matter. Quat. Res. 62, 183–193. https://doi.org/10.1016/j.yqres.2004.06.003.

Prentice, I.C., Harrison, S.P., 2009. Ecosystem effects of CO_2 concentration: evidence from past climates. Clim. Past 5, 297–307.

Punyasena, S., Mayle, F., McElwain, J., 2008. Quantitative estimates of glacial and Holocene temperature and precipitation change in lowland Amazonian Bolivia. Geology 36, 667–670.

Rowe, H., Hughes, N., Robinson, K., 2012. The quantification and application of handheld energy-dispersive x-ray fluorescence (ED-XRF) in mudrock chemostratigraphy and geochemistry. Chem. Geol. 324, 122–131.

Victoria, R.L., Fernandes, F., Martinelli, L.A., Piccolo, M.C., Camargo, P.B., Trumbore, S., 1995. Past vegetation changes in the Brazilian Pantanal arboreal–grassy savanna ecotone by using carbon isotopes in the soil organic matter. Glob. Change Biol. 1 (3), 165–171.

Wang, X., Edwards, R.L., Auler, A.S., Cheng, H., Kong, X., Wang, Y., Cruz, F.W., Dorale, J.A., Chiang, H.-W., 2017. Hydroclimate changes across the Amazon lowlands over the past 45,000 years. Nature 541, 204–207.

Ward, B.W., Wong, C.I., Novello, V.N., McGee, D., Santos, R.V., Silva, L.C.R., Cruz, F.W., Wang, X., Edwards, R.L., Cheng, H., 2019. Reconstruction of Holocene coupling between the South American Monsoon System and local moisture variability from speleothem $\delta^{18}O$ and $^{87}Sr/^{86}Sr$ records. Quat. Sci. Rev. 210, 51–63.

Weber, M., Scholz, D., Schröder-Ritzrau, A., Deininger, M., Spötl, C., Lugli, F., Mertz-Kraus, R., Jochum, K.P., Fohlmeister, J., Stumpf, C.F., Riechelmann, D.F.C., 2018. Evidence of warm and humid interstadials in central Europe during early MIS 3 revealed by a multi-proxy speleothem record. Quat. Sci. Rev. 200, 276–286.

Whitney, B.S., Punyasena, S.W., Mann, D.G., Metcalfe, S., 2011. A 45 kyr palaeoclimate record from the lowland interior of tropical South America. Palaeogeogr. Palaeoclimatol. Palaeoecol. 307, 177–192. https://doi.org/10.1016/j.palaeo.2011.05.012.

Woillez, M., Kageyama, M., Krinner, G., Viovy, N., Woillez, M., Kageyama, M., Krinner, G., Viovy, N., 2011. Impact of CO_2 and climate on the Last Glacial Maximum vegetation: results from the ORCHIDEE/IPSL models. Clim. Past 7, 557–577. https://doi.org/10.5194/cp-7-557-2011.

Wortham, B.E., Wong, C.I., Silva, L.C.R., Mcgee, D., Montañez, P., Rasbury, E.T., Cooper, K.M., Sharp, W.D., Glessner, J.J.G., Santos, R.V., 2017. Assessing response of local moisture conditions in central Brazil to variability in regional monsoon intensity using speleothem $^{87}Sr/^{86}Sr$ values. Earth Planet. Sci. Lett. 463, 310–332. https://doi.org/10.1016/j.epsl.2017.01.034.